




This is the **accepted version** of the article:

Serna, Naroa; Sanchez, Julieta M.; Unzueta Elorza, Ugutz; [et al.]. «Recruiting potent membrane penetrability in tumor cell-targeted protein-only nanoparticles». *Nanotechnology*, Vol. 30, Issue 11 (March 2019), art. 115101. DOI 10.1088/1361-6528/aaf959

This version is available at <https://ddd.uab.cat/record/233728>

under the terms of the  **CC BY** COPYRIGHT license

Recruiting potent membrane penetrability in tumor cell-targeted protein-only nanoparticles

Naroa Serna ^{1,2,3}, Julieta M. Sánchez ^{1,2,4}, Ugutz Unzueta ^{3,5}, Laura Sánchez-García ^{1,2,3}, Alejandro Sánchez-Chardi ⁶, Ramón Mangués ^{3,5}, Esther Vázquez ^{1,2,3*}, Antonio Villaverde ^{1,2,3*}

¹ Institut de Biotecnologia i de Biomedicina, Universitat Autònoma de Barcelona, Bellaterra, 08193 Barcelona, Spain

² Departament de Genètica i de Microbiologia, Universitat Autònoma de Barcelona, Bellaterra, 08193 Barcelona, Spain

³ CIBER de Bioingeniería, Biomateriales y Nanomedicina (CIBER-BBN), Bellaterra, 08193 Barcelona, Spain

⁴ Instituto de Investigaciones Biológicas y Tecnológicas (IIBYT) (CONICET-Universidad Nacional de Córdoba). ICTA & Cátedra de Química Biológica, Departamento de Química, FCEyN, UNC. Av. Velez Sarsfield 1611, X 5016GCA Córdoba, Argentina

⁵ Biomedical Research Institute Sant Pau (IIB-Sant Pau) and Josep Carreras Research Institute, Hospital de la Santa Creu i Sant Pau, 08025 Barcelona, Spain

⁶ Servei de Microscòpia, Universitat Autònoma de Barcelona, Bellaterra, 08193 Barcelona, Spain

Keywords: recombinant proteins; nanoparticles; self-assembling; protein engineering; cell targeting; antitumoral drugs

Abstract

The membrane pore-forming activities of the antimicrobial peptide GWH1 have been evaluated in combination with the CXCR4-binding properties of the peptide T22, in self-assembling protein nanoparticles with high clinical potential. The resulting materials, of 25 nm in size and with regular morphologies, show a dramatically improved cell penetrability into CXCR4⁺ cells (more than 10-fold) and enhanced endosomal escape (the lysosomal degradation dropping from 90 % to 50 %), when compared with equivalent protein nanoparticles lacking GWH1. These data reveal that GWH1 retains its potent membrane activity in form of nanostructured protein complexes. On the other hand, the specificity of T22 in the CXCR4 receptor binding is subsequently minimized but, unexpectedly, not abolished by the presence of the antimicrobial peptide. The functional combination T22-GWH1 results in 30 % of the nanoparticles entering cells via CXCR4 while also exploiting pore-based uptake. Such functional materials are capable to selectively deliver highly potent cytotoxic drugs upon chemical conjugation, promoting CXCR4-dependent cell death. These data support the further development of GWH1-empowered cell-targeted proteins as nanoscale drug carriers for precision medicines. This is a very promising approach to overcome lysosomal degradation of protein nanostructured materials with therapeutic value.

Introduction

Cell-targeted drug delivery requires appropriate nanoscale vehicles (usually nanoparticles) for the generation of nanoconjugates [1]. These carriers have to be functionalized with appropriate ligands (usually peptides or proteins) that selectively bind to cell surface receptors overexpressed in target cells [2]. Selective delivery is specially desired in oncology, in which conventional therapy is majorly based on the systemic administration of untargeted chemotherapeutic drugs, associated to severe life-threatening side toxicity [3-7]. A nanoscale size of the conjugate, ranging from 10 to 100 nm, allows exploiting the enhanced permeability and retention (EPR) effect (based on the higher blood vessel permeability in tumoral tissues) while avoiding renal clearance (with a cut-off around 6-8 nm) and undesired aggregation in lung capillaries [8]. A diversity of materials is explored as nanoscale drug carriers including polymers, ceramics, metals and carbon nanotubes. The xenobiotic nature and potential toxicity of most of them pose severe concerns about their biosafety, at both individual and environmental levels [1, 9-18]. Contrarily, self-assembling proteins are promising, fully biocompatible nanostructured materials for drug delivery [19, 20]. The development of nanosized protein materials is strongly pushed by emerging nanobiotechnologies [20-24], that allow the engineering of proteins to confer self-assembling at the nanoscale. Being functionally versatile, proteins and protein materials can perform complex activities such as precise cell targeting, by the incorporation of peptide ligands in modular polypeptides, that act as building blocks of nanoscale entities [25]. In this context, T22 is a highly selective cationic ligand of the cytokine receptor CXCR4, that is overexpressed in about 20 human neoplasias and that correlates with aggressiveness and metastasis [26-32]. T22 promotes the endosomal-mediated internalization of non-amyloid, self-assembling protein nanoparticles (formed by the T22-GFP-H6 fusion protein as building block), that result in the range size of 12 and 20 nm [33]. Selective T22-mediated binding and internalization result in a high level of specificity both *in vitro* and *in vivo* [34-36], and in an optimal biodistribution of the material in colorectal cancer animal models, when systemically administered [37]. In this context, T22-GFP-H6 nanoparticles have been recently used as potent nanocarriers of conventional antitumoral drugs [38], and closely related protein nanoparticles as vehicles for specific cytotoxic protein delivery in different cancer animal models [39, 40], both approaches with high therapeutic impact.

In protein-based nanoparticles, functional recruitment by protein fusion technologies [40-42] might be useful to enhance the penetrability of this construct (and similar nanoscale protein materials), which is now moderate, in order to improve its applicability as drug carrier. In this regard, poor endosomal escape and consequent lysosomal degradation

may be a critical bottleneck for T22-GFP-H6 to efficiently deliver cytotoxic drugs into the cytoplasm, as generically observed for proteins and confirmed in our laboratory for CXCR4-targeted constructs (U. Unzueta, unpublished data). Since self-assembling proteins are highly versatile materials, we have here studied the combined activity of T22 and that of a potent pore-forming protein, the antimicrobial peptide (AMP) GWH1, simultaneously displayed on the surface of protein nanoparticles. Although highly promising in nanomedical applications, the combination of cell-targeting peptides and enhancers of cell penetrability has been so far poorly studied, while it might offer a way to overcome lysosomal degradation and limited functionality in the target cell. The data presented here demonstrate that GWH1 shows potent endosomolytic activity that increases transfection efficiency of functionalized protein nanoparticles into the cytoplasm. Despite this fact, the CXCR4 binding specificity is conserved, although reduced, in these materials. The functional combination provided by the peptide pair is then a promising approach to enhance the performance of smart drug nanocarriers based on functional peptides.

Materials and methods

Nanoparticle production and characterization

Self-assembling modular proteins T22-GFP-H6 [34], T22-GWH1-GFP-H6 [42] and GWH1-GFP-H6 [43] (Figure 1 A) have been described elsewhere. T22 is a powerful ligand of the cell surface cytokine receptor CXCR4 [34], overexpressed in more than 20 aggressive human neoplasias [28, 30, 44] and that acts as a highly convenient target for the precision delivery of antitumoral and antimetastatic drugs [38-40]. T22 mediates the endosomal internalization of fusion proteins that contain the peptide, in CXCR4⁺ cells, both *in vitro* and *in vivo* [34, 36]. These gene fusions were expressed from the plasmid pET22b in *Escherichia coli* Origami B (BL21, *OmpT*⁻, *Lon*⁻, *TrxB*⁻, *Gor*⁻, Novagen) under standard conditions [37]. Cells were disrupted in a French Press (Thermo FA-078A) at 1200 psi to obtain the soluble fraction. Protein purification was carried out through the His-tag by Immobilized Metal Affinity Chromatography (IMAC) using a HiTrap Chelating HP 1 ml column (GE Healthcare) with an AKTA purifier FPLC (GE Healthcare) [45]. Proteins were finally dialyzed against sodium bicarbonate buffer with salt (166 mM NaHCO₃ pH 8 + 333 mM NaCl). Protein purity and integrity were checked by mass spectrometry (MALDI-TOF) and protein amounts by the Bradford assay.

Morphometric (size and shape) and ultrastructural characterization

The volume size distribution of nanoparticles was determined by dynamic light scattering (DLS) at 633 nm (Zetasizer Nano ZS, Malvern Instruments Limited, Malvern). The surface charge of proteins was assessed by zeta potential (Zp). Zp was measured at 25 °C and 633 nm, and DTS1070-folded capillary cell was used as sample container (Zetasizer Nano ZS, Malvern Instruments Limited). For quantitative analyses, three replicas of each sample were analyzed and the error in the measurements were estimated. Shape of nanoparticles was evaluated with a Field emission scanning electron microscopy (FESEM) Zeiss Merlin (Zeiss) equipped with a high resolution in-lens secondary electron detector and operating at 1 kV. To estimate the molecular mass of the purified nanoparticles size exclusion chromatography (SEC) was performed on a Superdex 200 10/300 column (GE Healthcare). The column was previously calibrated with molecular-mass standards (GE Healthcare) and injected protein nanoparticles (250 µl each) were eluted with a sodium bicarbonate buffer.

Membrane preparation and Circular dichroism (CD)

Multilamellar vesicles were prepared by evaporating, under a stream of nitrogen, chloroform:methanol (2:1 v/v) from a solution of pure egg phosphatidyl choline (EPC) (Sigma Aldrich). The dry lipid was resuspended in buffer at 1 mg/ml by repeating six

consecutive cycles of heating for 2 min at 21 °C (a temperature above the phospholipid T_c) and vortexing for 1 min. In these conditions, EPC self-aggregates into multilamellar vesicles (MLVs) [46]. Small unilamellar vesicles (SUVs) were prepared using a high intensity sonicator Branson sonifier 450, with 3 mm-diameter titanium probe. 1 ml of MLVs dispersion containing 4 mg/ml of EPC maintained on ice was sonicated for six cycles of 20 sec, each one with 50% pulses (0.5 sec on and 0.5 sec off) The last sample was centrifuged at 15000 g x 15 min to discard big aggregates and titanium particles.

Far-UV CD was measured at 25°C in a Jasco J-715 spectropolarimeter to assess secondary structure information. The concentration of T22-GFP-H6 and T22-GWH1-GFP-H6 was adjusted to 0.2 mg/ml in a buffer solution of 166 mM carbonate-bicarbonate at pH 8 and 333 mM NaCl. The protein spectrum was measured in the absence or the presence of small unilamellar vesicles (SUVs) (phosphatidylcholine at 0.5 and 1 mg/ml). Samples were analysed with a 1 mm path length cuvette. CD spectra were obtained over a wavelength range of 190-240 nm at a scan rate of 50 nm/min a response of 1 sec and a bandwidth of 1 nm. Six scans were accumulated.

Cell culture and cell viability assay

Cervical and colorectal cancer cell lines were used to study the performance of recombinant proteins *in vitro* (CXCR4⁺ HeLa, CXCR4⁺ SW1417 and CXCR4⁻ SW1417 cells). HeLa cells were cultured in MEM Alpha (Minimum Essential Medium) supplemented with 10 % fetal calf serum (Gibco) at 37 °C and 5 % CO₂ in a humidified atmosphere whereas SW1417 cells in Dulbecco's Modified Eagle's Medium (Gibco). To explore internalization and CXCR4 specific uptake of proteins, culture media was exchanged for serum-free Optipro medium (Gibco) supplemented with L-glutamine prior to the addition of nanoparticles. T22-GWH1-GFP-H6 and control T22-GFP-H6 and GWH1-GFP-H6 nanoparticles were added at 25 nM during 2 h in HeLa and SW1417 cells. Specific internalization through CXCR4 receptor was proved adding 1 h prior protein incubation a specific antagonist of CXCR4, AMD3100 at a ratio of 1:10. The CellTiter-Glo® Luminescent Cell Viability Assay (Promega) was used to determine the cytotoxicity of protein nanoparticles. For that, HeLa cells were plated in opaque-walled 96-well plates at 3,500 cells/well in DMEM supplemented with 10 % fetal calf serum for 24 h at 37 °C until reaching 70 % confluence. Then, cells were incubated in presence of 2, 4, 8, 12 and 24 µM nanoparticles during 48 h at 37°C. Subsequently, 100 µl of the single reagent (CellTiter-Glo® Reagent) was added directly to cultured cells and the plates were measured in the Multilabel Plate Reader VICTOR3 (PerkinElmer).

Internalization and endosomal degradation assays

To determine the threshold concentration for endosomal membrane destabilization, T22-GWH1-GFP-H6 and control T22-GFP-H6 and GWH1-GFP-H6 nanoparticles were added at 0.5, 1, 2, 3 and 4 μ M and left for 24h. To analyze endosomal escape of proteins, HeLa cells were treated with chloroquine (10 μ M) for 24h. Chloroquine induces vesicular rupture through protonation, in the acidic environment of late endosomes and lysosomes [47, 48]. Since chloroquine allows endosomal release and prevents lysosomal proteolysis [49], the increase in the intracellular material upon chloroquine addition is observed as indicative of the extent of lysosomal degradation of internalized protein in absence of the drug.

The uptake kinetics were recorded by exposing cells to nanoparticles at 1 and 4 μ M for 2, 5.5, 11, 16, 21 and 24 h prior to fluorescence measurement. Again, chloroquine was used for the determination of endosomal escape. Internalization was analyzed by detaching the cells with 1 mg/ml trypsin-EDTA (Gibco®) for 15 min, in a protocol specifically designed to remove externally attached protein [50]. The samples were analyzed by a FACS-Canto system (Becton Dickinson) using a 15 mW air-cooled argon ion laser at 488 nm excitation. All experiments were performed in duplicate. Fluorescence data recorded by cytometry were corrected by the specific fluorescence of the protein to render comparative units in terms of protein amount. The specific fluorescence was previously determined by a Varian Cary Eclipse fluorescence spectrophotometer (Agilent Technologies) at 523 nm using an excitation wavelength of 488 nm.

Confocal laser scanning microscopy

For confocal microscopy, HeLa cells were grown on Mat-Tek plates (MatTek Corporation). Upon exposure to nanoparticles at 4 μ M for 24 h, cell nuclei were labelled with CellMask™ Deep Red (ThermoFischer) for 10 min at room temperature. Cells were then washed in PBS (Sigma-Aldrich Chemie GmbH). Live cells were recorded with a TCS-SP5 confocal laser scanning microscope (Leica Microsystems) using 63x (1.4 NA) oil immersion objective lenses. Hoechst 33342 labelled DNA was excited with a blue diode (405 nm) and detected in the 415-460 nm range. GFP-proteins were excited with an Ar laser (488 nm) and detected in the 525-545 nm range. CellMask was excited with a HeNe laser (633 nm) and detected in the 650-775 nm range. The confocal pinhole was set to 1 Airy unit and z-stacks acquisition intervals were selected to satisfy Nyquist sampling

criteria. Three-dimensional images were obtained using the Surpass Module in Imaris X64 v.7.2.1. software (Bitplane).

Synthesis and characterization of the T22-GWH1-GFP-H6-Auristatin nanoconjugate

The T22-GWH1-GFP-H6-Auristatine nanoconjugate (T22-GWH1-GFP-H6-A) was synthesized by covalent binding of the protein nanoparticle and Auristatin. The final conjugate was obtained by reacting maleimide groups of Auristatin with primary amines of nanoparticles (like lysine and arginine sidechains) favoured at pH = 8. The quality analysis of the conjugation was performed by MALDI-TOF spectra. The molecular mass of the T22-GWH1-GFP-H6-A carrying from 7 to 14 auristatin molecules (911 Da each) was identified by mass spectrometry. Next, we studied T22-GWH1-GFP-H6-A cytotoxic activity measuring cell viability and using the CellTiter-Glo® Luminescent Cell Viability Assay (Promega), following manufacturer recommendations. To that purpose, we exposed CXCR4⁺ HeLa cells to T22-GWH1-GFP-H6- α or T22-GWH1-GFP-H6- β compared to equimolecular concentrations of T22-GFP-H6-A or T22-GWH1-GFP-H6.

Statistics

All the experiments were performed in triplicate. One-way ANOVA, followed by least significant difference (LSD) method was used for multiple comparisons. Pairwise comparisons were performed using Student-t tests. Statistical differences (indicated as * in the Figures) were assumed at $p < 0.01$. Microsoft Excel was used for all statistical analyses.

Results

T22-GWH1-GFP-H6 (Figure 1A) contains the AMP GWH1 inserted as an additional module between the N-terminal CXCR4 ligand T22, and the core GFP. This protein, as well as the related constructs T22-GFP-H6 and GWH1-GFP-H6 (Figure 1A), form regular nanoparticles with a toroid-like morphology, because of the cationic character of the N-terminal region [51]. These materials show distinguishable Z potential values and nanoscale sizes (Figure 1A, B). In particular, T22-GWH1-GFP-H6 organizes as structures sizing 25 nm in average, being larger than the parental T22-GFP-H6 (12 nm) and smaller than the shorter GWH1-GFP-H6 (47 nm). SEC analysis of the three materials revealed different elution peaks, from which we estimated the structural composition of the particles in 31, 11 and 45 monomers respectively. The value for T22-GFP-H6 (formed by 11 building blocks), fits reasonably well with a previous *in silico* modelling of the oligomeric nanoparticle, that predicted the material being composed by 10 regularly accommodated GFP monomers [37].

We were interested in knowing if GWH1, a pore-forming peptide, might enhance the penetrability of the protein construct mediated by the specific interaction between T22 and CXCR4, upon endosomal membrane destabilization. GWH1 exerts its cytolytic activity by folding into an amphipathic helix upon selective binding and insertion into the target membrane. In order to investigate whether the addition of the T22 moiety and the nanoparticulated form itself might affect the α -helical structures, we measured the peptide conformation by circular dichroism (CD) in the absence or the presence of small unilamellar vesicles (SUVs). The T22-GWH1-GFP-H6-spectrum in the absence of SUVs shows a β -sheet pattern corresponding to the expected beta-barrel structure of the GFP (Figure 2A), with a minimum around 218 nm [52]. By contrast, when these nanoparticles interact with SUVs a qualitative change is observed in the DC spectrum in which the minimum moved to 222 nm (Figure 2A) corresponding to the appearance of novel helical conformation. Interestingly T22-GFP-H6 did not exhibit this qualitative change in CD spectrum as it interacted with SUVs (Figure 2A, bottom).

AMPs, as effective self-defence tools, exhibit a threshold concentration (called the lethal concentration) for their membrane activity on eukaryotic cells, below which no effect is observed [53]. This security level allows the antimicrobial activity at low concentrations, without harming own body cells. Since it had been previously described that GWH1 exhibits cytotoxic effects over cancer cells with a reported threshold ranging from 20 μ M to 250 μ M, we first determined the intrinsic cytotoxicity of T22-GWH1-GFP-H6 over

CXCR4⁺ HeLa cells. As observed (Figure 2B), T22-GWH1-GFP-H6 nanoparticles showed a dose-dependent cytotoxicity with a significant lethal concentration lower than the predicted for the GWH1 peptide alone. This cell killing effect, when properly targeted to tumoral tissues, has proved to be exploitable to design antitumoral drugs [42]. Under 8 μ M, no cytotoxicity was observed in HeLa cells upon exposure to T22-GWH1-GFP-H6 nanoparticles, and further analysis of cell penetrability and specificity were performed in a safe margin, up to 4 μ M.

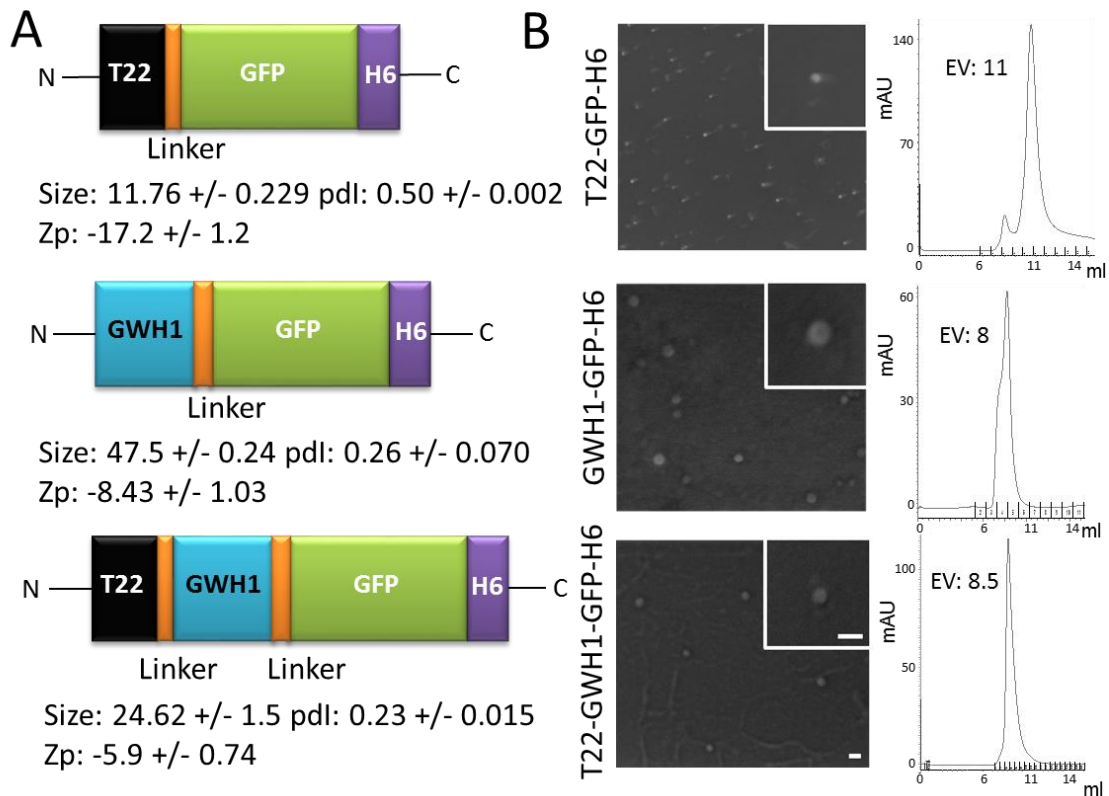


Figure 1. Features of GWH1-carrying nanoparticles. A. Modular organization of the set of protein building blocks used in this study. All the shown polypeptides self-assemble as fluorescent nanoparticles. Hydrodynamic size (in nm, measured by DLS) and polydispersity index (pdl) are shown at the bottom of each cartoon and Z-potential (Zp) of the nanoparticles (in mV) are also indicated. B. FESEM examination and size-exclusion chromatograms of purified nanoparticles monitored by UV detector at 280 nm. Bars indicate 50 nm, and all images have the same magnification. EV indicates the elution volume.

Then, endosomal escape promoted by GWH1 was evaluated by comparison between T22-GWH1-GFP-H6 and its parental T22-GFP-H6. As observed (Figure 3A), over 1.5 μM , T22-GWH1-GFP-H6 is dramatically more efficient than T22-GFP-H6 in escaping the endosome, suggesting a threshold concentration for endosomal membrane destabilization. This action cannot be performed by the control nanoparticle GWH1-GFP-H6, which lacks the cell surface ligand (T22) for internalization. Such endosomal escape protects the 40 % of the internalized protein nanoparticles from lysosomal degradation (Figure 3B), that is responsible for the destruction of most T22-GFP-H6. Interestingly, the presence of GWH1 impairs, contrarily, the CXCR4-dependence in the uptake of the protein materials (Figure 3C) but it does not abort it. Less than 2 % of T22-GFP-H6 enters target cells in the presence of the CXCR4 antagonist AMD3100, while almost 70 % of T22-GWH1-GFP-H6 penetrates HeLa cells under the same conditions (Figure 3C).

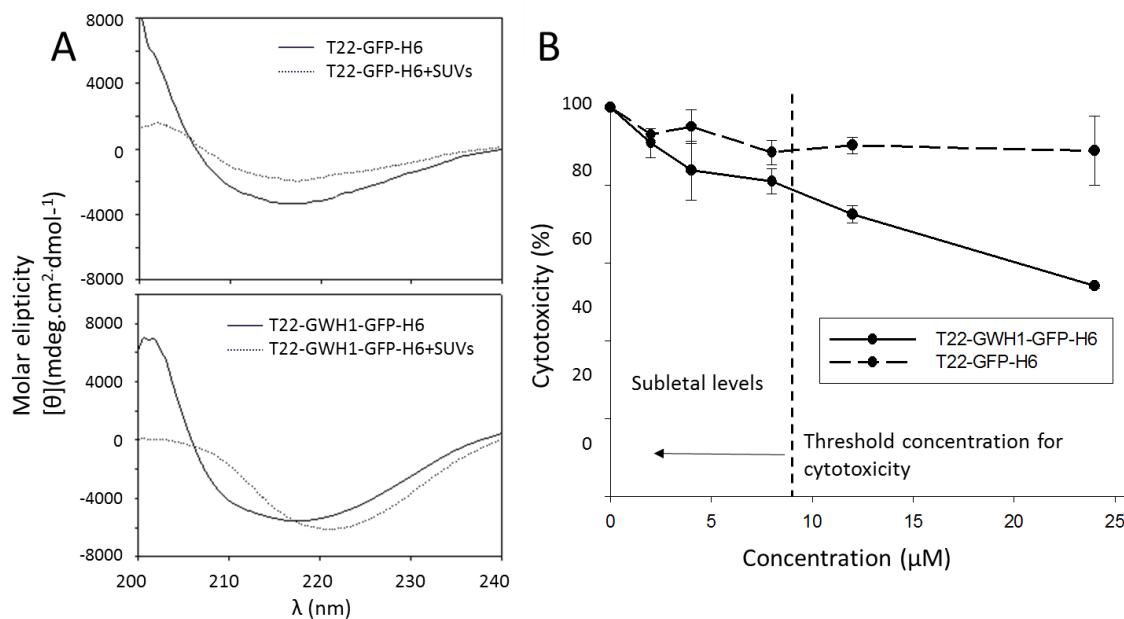


Figure 2. Interaction of GWH1-containing nanoparticles with cell membranes. A. T22-GWH1-GFP-H6 and T22-GFP-H6 CD spectra at wavelength range of 200. 240 nm. In the absence of SUVs, both spectra of proteins indicate the occurrence of β -sheet conformation. The CD spectra of T22-GWH1-GFP-H6, in presence of membranes, shows the appearance of the helical content. B. Intrinsic cytotoxicity on HeLa cells imposed by the AMP GWH1. Cells were incubated in presence of 2, 4, 8, 12 and 24 μM of protein assembled as nanoparticles during 48 h. T22-GFP-H6 does not show any biological effect at these doses. A threshold for GWH1 toxicity is shown

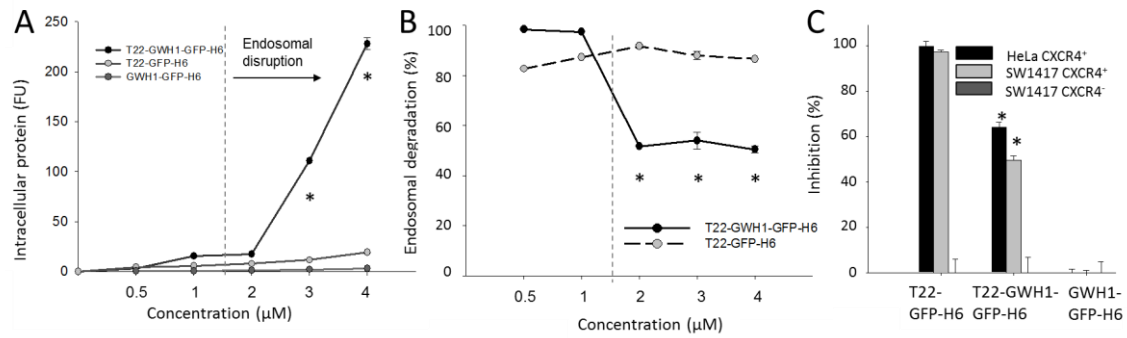


Figure 3. Cell penetration and endosomal escape of GWH1-containing nanoparticles. A. Cell internalization of GWH1-empowered nanoparticles measured through intracellular fluorescence, after a harsh trypsin treatment to remove external material. A threshold for the endosomal escape properties is shown at 1.5 μM . FU are fluorescence units. B. Fraction of internalized protein degraded in the endosomes, as measured by chloroquine addition. Cells were incubated in the absence and in the presence of GWH1-empowered nanoparticles. C. Specificity of CXCR4-mediated internalization of nanoparticles added at 25 nM visualized through the fraction of protein internalization inhibited by the CXCR4 antagonist, AMD3100 [54-56], incubated 1 h prior to protein treatment at a ratio of 1:10. * indicates significant differences between T22-GWH1-GFP-H6 data and that of the other proteins.

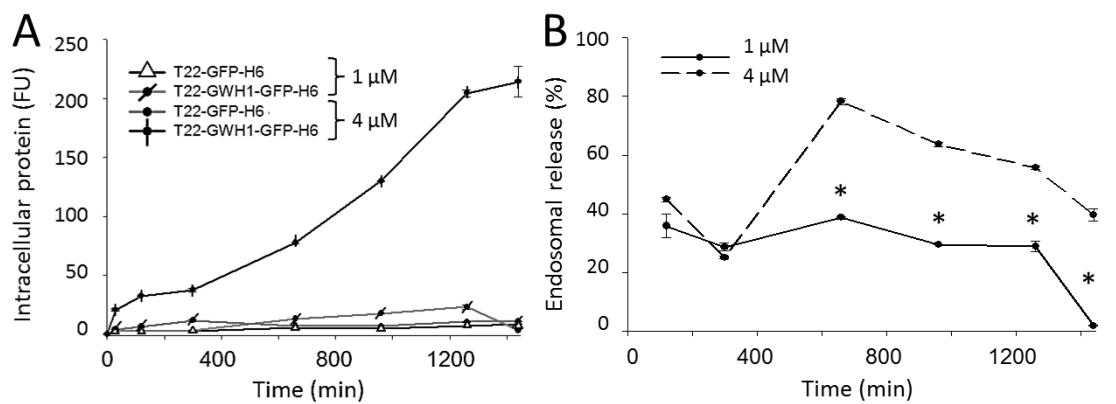


Figure 4. Dynamics of cell penetration of GWH1-containing nanoparticles. A. Kinetics of cell penetration of GWH1-empowered nanoparticles. Relative amounts of intracellular nanoparticles penetrating HeLa cells at different times after exposure (at 2 different concentrations). B. Endosomal release of T22-GWH1-GFP-H6 under the same conditions. * indicates significant differences between T22-GWH1-GFP-H6 data and that of the other proteins.

In accordance to the obtained results, at a concentration (1 μM) in which GWH1 does not promote endosomal escape, the cell uptake of T22-GWH1-GFP-H6 is slightly higher than that of the parental T22-GFP-H6 (Figure 4A). The uptake slows down at about 5 h,

reaching a steady constant intracellular concentration during 24 h. At a concentration above that threshold (4 μM), however, the penetration of T22-GWH1-GFP-H6 is extremely efficient. The amount of intracellular protein keeps increasing, without reaching any plateau at least during 24 h of exposure. During this experiment time, T22-GWH1-GFP-H6 is majorly degraded at 1 μM , but only 60 % of the material is destroyed at 24 h in the endosomes at 4 μM (Figure 4B). This observation confirms again, the endosomal escape of the nanoparticles promoted by GWH1. Under this situation, most of T22-GWH1-GFP-H6 is found homogenously distributed by the cell cytoplasm, while the parental T22-GFP-H6 is majorly concentrated in a perinuclear region, as dissected by 3D confocal reconstructions (Figure 5A). The perinuclear localization of T22-GFP-H6 fits with previous data that suggested a strong endosomal retention of this material [34]. The broadest intracellular distribution of T22-GWH1-GFP-H6 was confirmed by wide 2D confocal imaging of larger areas of cultured cells, at different magnifications (Figure 5B).

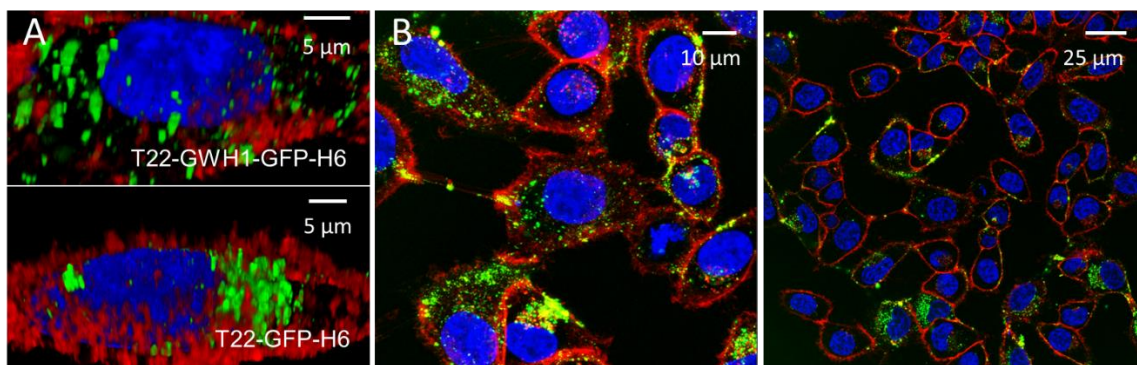


Figure 5. Intracellular localization and fate of protein nanoparticles. A. 3D confocal reconstructions of cultured HeLa cells exposed to 4 μM of GWH1-empowered nanoparticles and the control T22-GFP-H6. Blue label corresponds to the nucleus, red label to membranes and green label is the natural fluorescence of the nanoparticles. B. Broad confocal fields, at different magnifications, showing the intracellular localization of T22-GWH1-GFP-H6 homogenously distributed by the cell cytoplasm. All images were taken 24 h after exposure.

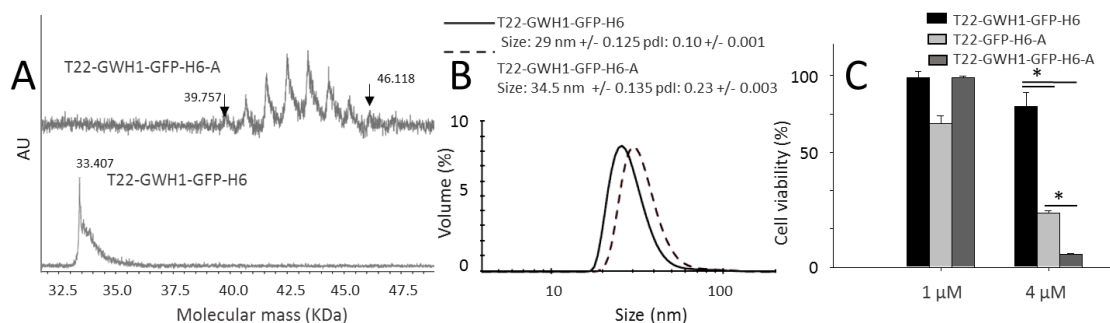


Figure 6. Characterization of T22-GWH1-GFP-H6-Auristatin nanoconjugates. A. Mass spectrometry of T22-GWH1-GFP-H6-Auristatin (labelled as A) upon chemical conjugation. Eight peaks were identified corresponding to nanoparticles with seven to fourteen attached drug molecules. Flanking peaks are indicated with arrows, and also their molecular masses. The non-labelled peaks correspond to molecular masses of 40.682, 41.601, 42.500, 43.413, 44.320 and 45.244 KDa respectively. At the bottom, the spectrum of drug-free nanoparticles. B. Hydrodynamic size distribution of T22-GWH1-GFP-H6-A nanoconjugate compared to the drug-free nanoparticle. C. Reduction in cell viability of HeLa cells exposed to T22-GWH1-GFP-H6-A for 48 h, as compared to T22-GFP-H6-A and T22-GWH1-GFP-H6. * indicates significant differences between T22-GWH1-GFP-H6-A data and that of the other proteins.

The high cell penetrability and improved endosomal escape conferred by the AMP to the protein nanoparticles, combined with the significant level of CXCR4 selectivity (Figure 3, 4 and 5) prompted us to explore its potentiality as vehicles for targeted drug delivery, and therefore their potentiality for clinical applications. For that, we chemically coupled the antitumoral drug Auristatin to T22-GWH1-GFP-H6, and explored the ability of the nanoconjugate (T22-GWH1-GFP-H6-A) to deliver the drug in the cell cytoplasm. Auristatin is potent antimitotic peptide derived from the mollusc *Dolabella auricularia*, with applicability in targeted therapies in a spectrum of tumors [57]. The chemical conjugation rendered a narrow spectrum of nanoconjugates ranging from 7 to 14 drug molecules per nanoparticle, as determined by MALDI (Figure 6 A), and it slightly modified the volume and Zp of the materials (Figure 6B). When CXCR4⁺ cells were exposed to drug-loaded nanoparticles, a dramatic impact on cell viability was observed (Figure 6C). Importantly, the nanoparticle version lacking the AMP (T22-GFP-H6-A) was less efficient in promoting cell death (Figure 6C), confirming again the positive impact of this peptide in the release of the whole complex, including the drug, to the cytoplasm.

Discussion

Protein-based drugs are of high interest in molecular medicines as they can be produced among a spectrum of cell factories by simple recombinant DNA technologies [58]. In cancer therapies, modular approaches based on fusion protein engineering [41] allow recruiting, in single chain polypeptides, diverse functions required for efficient cell targeting, internalization and endosomal escape, that are encoded by proteins or protein domains [25, 59]. Self-assembling, that can be provided by short peptide stretches [20], allows the proteins being presented as regular oligomers within the nanoscale size, a presentation that enhances their tumoral accumulation by physical mechanisms linked to the EPR [8]. In a step further beyond the simple protein-drug association principles (on which Abraxane® is based [60]), nanostructured, cell targeted proteins can be ideal vehicles for drug targeting in cancer therapy in form of drug nanoconjugates [3]. We have here tested the combination of the AMP GWH1 [61], a potent membrane pore former, with T22 [34], a potent CXCR4 ligand, in protein-only CXCR4-targeted nanoparticles, regarding efficiency and specificity of CXCR4⁺ cell binding and penetrability. GWH1 is a synthetic AMP designed to show enhanced antimicrobial activity while reduced cell killing activity on normal eukaryotic cells, such as 3T3 fibroblasts [62] or erythrocytes (with low haemolytic activity) [63]. It also shows improved selectivity for surface binding and killing of cancer cells as compared to normal cells, because of similarly to bacteria, their membrane is enriched in anionic components [64]. GWH1 exerts its cytolytic activity by folding into an amphipathic helix upon selectively binding and insertion into the target membrane, leading to breakdown of the membrane structure, thus causing leakage of cell contents, finally resulting in cell death. Being used as a synthetic peptide alone, GWH1 is fully functional in form of fusion proteins [43], what opens the door to consider its inclusion in multifunctional constructs. The combination of pore-forming and cell-targeting agents, despite their obvious interest in cancer therapies, has not been systematically explored.

In this context, we have demonstrated here that the accommodation of GWH1 in longer modular polypeptides containing the cationic CXCR4 ligand T22 (Figure 1 A) does not affect neither the functionality of GWH1 nor the ability of the T22- and H6-empowered proteins to form regular nanoparticles (Figure 1A). Moreover, a clear membrane-disrupting ability of T22-GWH1-GFP-H6 was shown over cancer cells with the expected threshold concentration (Figure 2), indicating the ability of GWH1 to create pores even in a nanoparticulated version. This fact can be obviously exploited to construct therapeutic protein materials based on functional recruitment, through simple fusion technologies. Interestingly, at sub-lethal concentrations, the GWH1 module enhances

rapid and effective translocation of T22-GWH1-GFP-H6 nanoparticles from the endocytic vesicles into cytoplasm, when comparing with the parenteral T22-GFP-H6 (Figure 3). Interestingly, despite its observable endosomolytic activity, GWH1 does not promote release from vesicles into the cytoplasm except when administered at concentrations compatible with molecular models currently proposed for antimicrobial sequences and the need of a threshold concentration for pore formation [53, 65, 66]. In this context, a punctuate fluorescence pattern was observed for internalized T22-GFP-H6 (Figure 5), indicating endosome permanence. In contrast, a different intracellular fluorescence pattern was shown by T22-GWH1-GFP-H6, characterized by a more homogeneous distribution of the material in the cytoplasm, consistent with the lysosomal release of a significant fraction of the recombinant cargo (Figure 5).

Interestingly, membrane pore formation, although a fully unspecific and very efficient process, does not abort the specific CXCR4-dependent cell penetration mediated by T22. CXCR4 specificity is however reduced by the presence of GWH1 in the protein constructs from more than 90 % to 30 % (Figure 3C). This indicates that enhanced cell penetrability though pore formation cannot be gained simultaneously to a high cell specificity, as previously observed when exploring the fusogenic peptide HA2 from the influenza virus hemagglutinin [67]. However, since the *in vivo* tumor targeting of antibody-drug conjugates has determined to be around 1 % [1, 18], 30 % of receptor specificity appears as still good data. In this context, the protein nanoparticles generated here and empowered with GWH1 have been efficiently loaded with the antitumoral drug Auristatin by chemical conjugation (Figure 6). The presence of the AMP in the material dramatically improved the cytotoxicity of the drug in the nanoconjugate when exposed to cultured CXCR4⁺ cell (Figure 6 C), when compared to the use of the parental T22-GFP-H6 as vehicle. These data, combined with the confocal microscopy imaging (Figure 5) and the experimental determining endosomal escape (Figure 3) demonstrate the endosomolytic properties of GWH1 when integrated, as a functional domain, in modular self-assembling proteins. Obviously, the clinical impact of pore formation combined with tumor cell targeting should be explored further. Since T22-based protein nanoconstructs have been recently shown extremely powerful for the precision delivery of chemical and protein antitumoral drugs [38-40, 42], the improvement of their intracellular trafficking properties, exploiting the functional versatility of protein materials, would be extremely desirable.

Conclusion

The obtained set of data stresses the strong value of membrane active peptides used as potential enhancers of drug penetrability and endosomal escape into target cells, when displayed in nanoscale supramolecular complexes. This has been proved here by the incorporation of GWH1 to a cell-targeted nanoscale protein vehicle through conventional protein engineering, generating a stable and functional nanomaterial. In addition, the presented results also point out that membrane pore formation does not preclude specific cell targeting mediated by a partner driver peptide, although the receptor specificity is reduced. In the current context of innovative drug design and the generation of smart nanoscale vehicles as delivery agents, the data presented in this study offer critical clues regarding the recruitment of appropriate functional agents based on recombinant proteins. The successful incorporation of membrane pore forming peptides into self-assembling functional proteins offers a powerful approach to overcome one of the major bottlenecks in the endosomal delivery of protein materials, namely lysosomal degradation.

Acknowledgments. This study has been funded by the Agencia Estatal de Investigación (AEI) and Fondo Europeo de Desarrollo Regional (FEDER) (grant BIO2016-76063-R, AEI/FEDER, UE), AGAUR (2017SGR-229) and CIBER-BBN (project NANOPROTHER) granted to AV, Marató de TV3 foundation (TV32013-3930) and ISCIII (PI15/00272 co-founding FEDER) to EV and ISCIII (PI15/00378 and PIE15/00028, co-founding FEDER), Marató de TV3 foundation (TV32013-2030) and AGAUR 2014-PROD0005 to RM. Specifically by the Protein Production Platform of CIBER-BBN/ IBB (<http://www.nanbiosis.es/unit/u1-protein-production-platform-ppp/>). We are indebted to SCAC (UAB) for cell culture facilities and assistance and to the Microscopy Service at the UAB. NS was supported by a predoctoral fellowship from the Government of Navarra, LSG was supported by AGAUR (2017FI_B100063), UU is supported by PERIS program from the health department of la Generalitat de Catalunya and JMS is a Career Investigator from CONICET. AV received an ICREA ACADEMIA award.

References

- [1] Duncan R, Gaspar R. Nanomedicine(s) under the microscope. *Molecular pharmaceutics* 2011;8:2101-41.

[2] Ozturk-Atar K, Eroglu H, Calis S. Novel advances in targeted drug delivery. *Journal of drug targeting* 2018;26:633-42.

[3] Mangues RV, E; Villaverde, A. Targeting in Cancer Therapies. *Medical Sciences* 2016;4:6.

[4] Moriarity A, O'Sullivan J, Kennedy J, Mehigan B, McCormick P. Current targeted therapies in the treatment of advanced colorectal cancer: a review. *Therapeutic advances in medical oncology* 2016;8:276-93.

[5] Yao VJ, D'Angelo S, Butler KS, Theron C, Smith TL, Marchio S, et al. Ligand-targeted theranostic nanomedicines against cancer. *Journal of controlled release : official journal of the Controlled Release Society* 2016;240:267-86.

[6] Kintzing JR, Filsinger Interrante MV, Cochran JR. Emerging Strategies for Developing Next-Generation Protein Therapeutics for Cancer Treatment. *Trends in pharmacological sciences* 2016;37:993-1008.

[7] Lee MS, Dees EC, Wang AZ. Nanoparticle-Delivered Chemotherapy: Old Drugs in New Packages. *Oncology* 2017;31:198-208.

[8] Shen J, Wolfram J, Ferrari M, Shen H. Taking the vehicle out of drug delivery. *Materials today* 2017;20:95-7.

[9] Durnev AD. Toxicology of nanoparticles. *Bulletin of experimental biology and medicine* 2008;145:72-4.

[10] Alexis F, Rhee JW, Richie JP, Radovic-Moreno AF, Langer R, Farokhzad OC. New frontiers in nanotechnology for cancer treatment. *Urologic oncology* 2008;26:74-85.

[11] Yildirimer L, Thanh NT, Loizidou M, Seifalian AM. Toxicology and clinical potential of nanoparticles. *Nano today* 2011;6:585-607.

[12] Sayes CM, Reed KL, Warheit DB. Nanoparticle toxicology: measurements of pulmonary hazard effects following exposures to nanoparticles. *Methods in molecular biology* 2011;726:313-24.

[13] Albanese A, Tang PS, Chan WC. The effect of nanoparticle size, shape, and surface chemistry on biological systems. *Annual review of biomedical engineering* 2012;14:1-16.

- [14] Elsaesser A, Howard CV. Toxicology of nanoparticles. *Advanced drug delivery reviews* 2012;64:129-37.
- [15] Wang AZ, Langer R, Farokhzad OC. Nanoparticle delivery of cancer drugs. *Annual review of medicine* 2012;63:185-98.
- [16] Shang L, Nienhaus K, Nienhaus GU. Engineered nanoparticles interacting with cells: size matters. *J Nanobiotechnology* 2014;12:5.
- [17] Haynes C. Editorial--analytical toxicology of nanoparticles. *The Analyst* 2014;139:868-9.
- [18] Stefan Wilhelm AJT, Qin Dai, Seiichi Ohta, Julie Audet, Harold F. Dvorak & Warren C. W. Chan. Analysis of nanoparticle delivery to tumours. *Nature Reviews Materials* 2016;1.
- [19] Corchero JL, Vazquez E, Garcia-Fruitos E, Ferrer-Miralles N, Villaverde A. Recombinant protein materials for bioengineering and nanomedicine. *Nanomedicine* 2014;9:2817-28.
- [20] Ferrer-Miralles N, Rodriguez-Carmona E, Corchero JL, Garcia-Fruitos E, Vazquez E, Villaverde A. Engineering protein self-assembling in protein-based nanomedicines for drug delivery and gene therapy. *Critical reviews in biotechnology* 2015;35:209-21.
- [21] Vazquez E, Villaverde A. Engineering building blocks for self-assembling protein nanoparticles. *Microbial cell factories* 2010;9:101.
- [22] Doll TAPF, Dey R, Burkhard P. Design and optimization of peptide nanoparticles. *J Nanobiotechnol* 2015;13.
- [23] Kumar VA, Wang BK, Kanahara SM. Rational design of fiber forming supramolecular structures. *Exp Biol Med* 2016;241:899-908.
- [24] Yeates TO, Liu Y, Laniado J. The design of symmetric protein nanomaterials comes of age in theory and practice. *Current opinion in structural biology* 2016;39:134-43.
- [25] Unzueta U, Cespedes MV, Vazquez E, Ferrer-Miralles N, Mangués R, Villaverde A. Towards protein-based viral mimetics for cancer therapies. *Trends in biotechnology* 2015;33:253-8.

- [26] Koshiba T, Hosotani R, Miyamoto Y, Ida J, Tsuji S, Nakajima S, et al. Expression of stromal cell-derived factor 1 and CXCR4 ligand receptor system in pancreatic cancer: a possible role for tumor progression. *Clinical cancer research : an official journal of the American Association for Cancer Research* 2000;6:3530-5.
- [27] Murakami T, Cardones AR, Hwang ST. Chemokine receptors and melanoma metastasis. *Journal of dermatological science* 2004;36:71-8.
- [28] Balkwill F. The significance of cancer cell expression of the chemokine receptor CXCR4. *Seminars in cancer biology* 2004;14:171-9.
- [29] Burger JA, Kipps TJ. CXCR4: a key receptor in the crosstalk between tumor cells and their microenvironment. *Blood* 2006;107:1761-7.
- [30] Kim J, Mori T, Chen SL, Amersi FF, Martinez SR, Kuo C, et al. Chemokine receptor CXCR4 expression in patients with melanoma and colorectal cancer liver metastases and the association with disease outcome. *Annals of surgery* 2006;244:113-20.
- [31] Barbieri F, Bajetto A, Florio T. Role of chemokine network in the development and progression of ovarian cancer: a potential novel pharmacological target. *Journal of oncology* 2010;2010:426956.
- [32] Weiss ID, Jacobson O. Molecular imaging of chemokine receptor CXCR4. *Theranostics* 2013;3:76-84.
- [33] Sanchez JM, Sanchez-Garcia L, Pesarrodonna M, Serna N, Sanchez-Chardi A, Unzueta U, et al. Conformational Conversion during Controlled Oligomerization into Nonamylogenic Protein Nanoparticles. *Biomacromolecules* 2018;19:3788-97.
- [34] Unzueta U, Cespedes MV, Ferrer-Miralles N, Casanova I, Cedano J, Corchero JL, et al. Intracellular CXCR4(+) cell targeting with T22-empowered protein-only nanoparticles. *International journal of nanomedicine* 2012;7:4533-44.
- [35] Cespedes MV, Unzueta U, Tatkiewicz W, Sanchez-Chardi A, Conchillo-Sole O, Alamo P, et al. In vivo architectonic stability of fully de novo designed protein-only nanoparticles. *ACS nano* 2014;8:4166-76.
- [36] Cespedes MV, Unzueta U, Alamo P, Gallardo A, Sala R, Casanova I, et al. Cancer-specific uptake of a liganded protein nanocarrier targeting aggressive CXCR4+

colorectal cancer models. *Nanomedicine : nanotechnology, biology, and medicine* 2016;12:1987-96.

[37] Rueda F, Cespedes MV, Conchillo-Sole O, Sanchez-Chardi A, Seras-Franzoso J, Cubarsi R, et al. Bottom-Up Instructive Quality Control in the Biofabrication of Smart Protein Materials. *Advanced materials* 2015;27:7816-22.

[38] Cespedes MV, Unzueta U, Avino A, Gallardo A, Alamo P, Sala R, et al. Selective depletion of metastatic stem cells as therapy for human colorectal cancer. *EMBO molecular medicine* 2018.

[39] Sanchez-Garcia L, Serna N, Alamo P, Sala R, Cespedes MV, Roldan M, et al. Self-assembling toxin-based nanoparticles as self-delivered antitumoral drugs. *Journal of controlled release : official journal of the Controlled Release Society* 2018;274:81-92.

[40] Diaz R, Pallares V, Cano-Garrido O, Serna N, Sanchez-Garcia L, Falgas A, et al. Selective CXCR4(+) Cancer Cell Targeting and Potent Antineoplastic Effect by a Nanostructured Version of Recombinant Ricin. *Small* 2018;14:e1800665.

[41] Vazquez E, Manges R, Villaverde A. Functional recruitment for drug delivery through protein-based nanotechnologies. *Nanomedicine* 2016;11:1333-6.

[42] Serna NC, M; Sánchez-García, L; Unzueta, U; Sala, R; Sánchez-Chardi, A; Cortés, F; Ferrer-Miralles, N; Manges, R; Vázquez, E; Villaverde, A. Peptide-Based Nanostructured Materials with Intrinsic Proapoptotic Activities in CXCR4+ Solid Tumors. *Advanced Functional Materials* 2017;27:1700919.

[43] Serna N, Sanchez-Garcia L, Sanchez-Chardi A, Unzueta U, Roldan M, Manges R, et al. Protein-only, antimicrobial peptide-containing recombinant nanoparticles with inherent built-in antibacterial activity. *Acta biomaterialia* 2017;60:256-63.

[44] Wang Y, Xie Y, Oupicky D. Potential of CXCR4/CXCL12 Chemokine Axis in Cancer Drug Delivery. *Current pharmacology reports* 2016;2:1-10.

[45] Pesarrodonna M, Crosas E, Cubarsi R, Sanchez-Chardi A, Saccardo P, Unzueta U, et al. Intrinsic functional and architectonic heterogeneity of tumor-targeted protein nanoparticles. *Nanoscale* 2017;9:6427-35.

- [46] Sanchez JM, Nolan V, Perillo MA. beta-galactosidase at the membrane-water interface: a case of an active enzyme with non-native conformation. *Colloids and surfaces B, Biointerfaces* 2013;108:1-7.
- [47] Varkouhi AK, Scholte M, Storm G, Haisma HJ. Endosomal escape pathways for delivery of biologicals. *Journal of controlled release : official journal of the Controlled Release Society* 2011;151:220-8.
- [48] Mellman I, Fuchs R, Helenius A. Acidification of the endocytic and exocytic pathways. *Annual review of biochemistry* 1986;55:663-700.
- [49] Fredericksen BL, Wei BL, Yao J, Luo T, Garcia JV. Inhibition of endosomal/lysosomal degradation increases the infectivity of human immunodeficiency virus. *Journal of virology* 2002;76:11440-6.
- [50] Richard JP, Melikov K, Vives E, Ramos C, Verbeure B, Gait MJ, et al. Cell-penetrating peptides. A reevaluation of the mechanism of cellular uptake. *The Journal of biological chemistry* 2003;278:585-90.
- [51] Unzueta U, Ferrer-Miralles N, Cedano J, Zikung X, Pesarrodona M, Saccardo P, et al. Non-amyloidogenic peptide tags for the regulatable self-assembling of protein-only nanoparticles. *Biomaterials* 2012;33:8714-22.
- [52] Fasman G. *Circular Dichroism and the Conformational Analysis of Biomolecules*. . New York Plenum Press. ; 1996.
- [53] Huang HW. Free energies of molecular bound states in lipid bilayers: lethal concentrations of antimicrobial peptides. *Biophys J* 2009;96:3263-72.
- [54] Kawaguchi A, Orba Y, Kimura T, Iha H, Ogata M, Tsuji T, et al. Inhibition of the SDF-1alpha-CXCR4 axis by the CXCR4 antagonist AMD3100 suppresses the migration of cultured cells from ATL patients and murine lymphoblastoid cells from HTLV-I Tax transgenic mice. *Blood* 2009;114:2961-8.
- [55] Kim HY, Hwang JY, Kim SW, Lee HJ, Yun HJ, Kim S, et al. The CXCR4 Antagonist AMD3100 Has Dual Effects on Survival and Proliferation of Myeloma Cells In Vitro. *Cancer research and treatment : official journal of Korean Cancer Association* 2010;42:225-34.

- [56] Song JS, Kang CM, Kang HH, Yoon HK, Kim YK, Kim KH, et al. Inhibitory effect of CXC chemokine receptor 4 antagonist AMD3100 on bleomycin induced murine pulmonary fibrosis. *Experimental & molecular medicine* 2010;42:465-72.
- [57] Lambert JM, Morris CQ. Antibody-Drug Conjugates (ADCs) for Personalized Treatment of Solid Tumors: A Review. *Advances in therapy* 2017;34:1015-35.
- [58] Sanchez-Garcia L, Martin L, Mangués R, Ferrer-Miralles N, Vazquez E, Villaverde A. Recombinant pharmaceuticals from microbial cells: a 2015 update. *Microbial cell factories* 2016;15:33.
- [59] Vazquez E, Ferrer-Miralles N, Mangués R, Corchero JL, Schwartz S, Jr., Villaverde A. Modular protein engineering in emerging cancer therapies. *Current pharmaceutical design* 2009;15:893-916.
- [60] Gradishar WJ. Albumin-bound paclitaxel: a next-generation taxane. *Expert opinion on pharmacotherapy* 2006;7:1041-53.
- [61] Felicio MR, Silva ON, Goncalves S, Santos NC, Franco OL. Peptides with Dual Antimicrobial and Anticancer Activities. *Frontiers in chemistry* 2017;5:5.
- [62] Chen YL, Li JH, Yu CY, Lin CJ, Chiu PH, Chen PW, et al. Novel cationic antimicrobial peptide GW-H1 induced caspase-dependent apoptosis of hepatocellular carcinoma cell lines. *Peptides* 2012;36:257-65.
- [63] Chou HT, Kuo TY, Chiang JC, Pei MJ, Yang WT, Yu HC, et al. Design and synthesis of cationic antimicrobial peptides with improved activity and selectivity against *Vibrio* spp. *International journal of antimicrobial agents* 2008;32:130-8.
- [64] Hoskin DW, Ramamoorthy A. Studies on anticancer activities of antimicrobial peptides. *Biochimica et biophysica acta* 2008;1778:357-75.
- [65] Lee MT, Hung WC, Chen FY, Huang HW. Many-body effect of antimicrobial peptides: on the correlation between lipid's spontaneous curvature and pore formation. *Biophys J* 2005;89:4006-16.
- [66] Hall K, Lee TH, Mechler AI, Swann MJ, Aguilar MI. Real-time measurement of membrane conformational states induced by antimicrobial peptides: balance between recovery and lysis. *Scientific reports* 2014;4:5479.

[67] Sanchez-Garcia L, Serna N, Mattanovich M, Cazzanelli P, Sanchez-Chardi A, Conchillo-Sole O, et al. The fusogenic peptide HA2 impairs selectivity of CXCR4-targeted protein nanoparticles. *Chemical communications* 2017;53:4565-8.